NASA TECHNICAL MEMORANDUM

NASA TM X-72693

NASA TM X-72693

(NASA-TM-X-72693) EFFECT OF WING-TIP DIHEDRAL ON THE LONGITUDINAL AND LATERAL AERODYNAMIC CHARACTERISTICS OF A SUPERSONIC CRUISE CONFIGURATION AT SUBSONIC SPEEDS (NASA) 42 p HC $4.00 CSCL 01A G3/02

N76-29156

Unclas 48696

EFFECT OF WING-TIP DIHEDRAL ON THE LONGITUDINAL AND LATERAL AERODYNAMIC CHARACTERISTICS OF A SUPERSONIC CRUISE CONFIGURATION AT SUBSONIC SPEEDS

By Karen E. Washburn, Purdue University and
Blair B. Gloss, NASA Langley Research Center

August 1976

NATIONAL AERONAUTICS AND SPACE ADMINISTRATION
LANGLEY RESEARCH CENTER, HAMPTON, VIRGINIA 23665

1. Report No. NASA TM X-72693	2. Government Accession No.	3. Recipient's Catalog No.
4. Title and Subtitle EFFECT OF WING-TIP DIHEDRAL ON THE LONGITUDINAL AND LATERAL AERODYNAMIC CHARACTERISTICS OF A SUPERSONIC CRUISE CONFIGURATION AT SUBSONIC SPEEDS		5. Report Date August 1976 6. Performing Organization Code
7. Author(s) Karen E. Washburn and Blair B. Gloss		8. Performing Organization Report No.
9. Performing Organization Name and Address NASA Langley Research Center Hampton, Virginia 23665		10. Work Unit No. 505-11-21-02 11. Contract or Grant No.
12. Sponsoring Agency Name and Address National Aeronautics and Space Administration Washington, DC 20546		13. Type of Report and Period Covered Technical Memorandum 14. Sponsoring Agency Code

15. Supplementary Notes

Final release of special information not suitable for formal publication.

16. Abstract

Force and moment data studies were conducted to determine the effect of wing-tip dihedral on the longitudinal and lateral aerodynamic characteristics of a supersonic cruise fighter configuration. Oil flow studies were also performed to investigate the model surface flow. Three models were tested: a flat (0^{0} dihedral) wing tip, a dihedral and an anhedral wing tip. The tests were conducted at the NASA Langley high-speed 7- by 10-foot wind tunnel.

17. Key Words (Suggested by Author(s))
Wing-Tip Dihedral
Supercruise
Vortex Lift

18. Distribution Statement
Unclassified-Unlimited

19. Security Classif. (of this report)	20. Security Classif. (of this page)	21. No. of Pages	22. Price*
Unclassified	Unclassified	40	$3.75

*For sale by the National Technical Information Service, Springfield, Virginia 22161

ABSTRACT

Force and moment data studies were conducted to determine the effect of wing-tip dihedral on the longitudinal and lateral aerodynamic characteristics of a supersonic cruise fighter configuration. Oil flow studies were also performed to investigate the model surface flow. Three models were tested: a flat (0° dihedral) wing tip, a dihedral and an anhedral wing tip. The tests were conducted at the NASA Langley high-speed 7- by 10-foot wind tunnel.

SUMMARY

Studies were conducted in the NASA Langley high-speed 7- by 10-foot wind tunnel to determine the effect of wing-tip dihedral on the longitudinal and lateral aerodynamic characteristics. Three cases were tested: a flat wing tip (with no spanwise camber), a dihedral and an anhedral wing tip configuration. Both force data and oil flow visualization results are presented. A comparison of theoretical and experimental results along with oil flow results indicate a complex vortex flow field.

Longitudinal force results for the three configurations show little change as the wing tips are varied. The anhedral model exhibits a slight improvement in lift and pitching moment. Lateral force data trends are similar for all three cases.

Due to the complexity of the vortex flow field, especially on the outer panels, further studies are recommended to investigate the effect of various leading edge sweeps and notch ratios in conjunction with wing-tip dihedral.

INTRODUCTION

Recent emphasis on the design of supersonic cruise fighter aircraft raises questions regarding the optimum method of providing adequate maneuvering performance for these highly swept, low aspect ratio wing aircraft at subsonic and transonic speeds. The design of such aircraft to provide satisfactory subsonic-transonic maneuvering performance may depend, to a large degree, on the use of the highly stable shed vortex system from the leading edge and subsequently, high levels of vortex lift. The simplicity, low structural weight, stability, and high levels of lift associated with this concept appear to offer an advantage over variable geometry maneuver systems.

Considerable theoretical studies of vortex lift based on the leading edge suction analogy, as well as experimental tests to verify the theories have been made (for example, references 1 and 2). In order that the lift resulting from the shed vortex system may be more effectively utilized, experimental studies have been conducted to define and further identify parameters affecting the formation and growth of the vortex system (references 3-6 for example).

Since some of the configurations envisioned for a supersonic cruise fighter utilize upswept wing tips, the present force and moment data study was conducted to determine the effects of wing-tip dihedral on the subsonic longitudinal and lateral-directional aerodynamic characteristics of a typical supersonic cruise fighter planform model with sharp leading edges. In addition, oil flow photographs were taken to study

the flow on the model surface. Three wing tips were studied including anhedral as well as dihedral.

SYMBOLS

The International System of Units, with the U.S. Customary Units presented in parentheses, is used for the physical quantities found in this paper. Measurements and calculations were made in the U.S. Customary Units. The data presented in this report are referred to the stability axis system, with the exception of the side force data, which is referred to the body axis system. The moment reference point was taken to be at the centerline station .683 m (2.41 ft.) aft of the nose.

b wing span, .660 m (2.17 ft.)

C_D drag coefficient, $\frac{\text{Drag}}{qS}$

C_L lift coefficient, $\frac{\text{Lift}}{qS}$

C_Y side-force coefficient, $\frac{\text{Side Force}}{qS}$

C_l rolling-moment coefficient, $\frac{\text{Rolling Moment}}{qSb}$

C_m pitching-moment coefficient, $\frac{\text{Pitching Moment}}{qS\bar{c}}$

C_n yawing moment coefficient, $\frac{\text{Yawing Moment}}{qSb}$

c_s leading-edge section suction force coefficient, $\frac{\text{Section Suction Force}}{qc}$

c stream wise chord

$\bar{c}$ wing reference chord, .369 m (1.21 ft.)

M free-stream Mach number

q free-stream dynamic pressure, 1915.2 N/m^2 (40 lb/ft^2)

S reference area of projected planform view, .0229 m^2 (2.41 ft^2)

y spanwise distance from centerline, cm(in)

α angle of attack, degrees

β angle of sideslip, degrees

η nondimensional spanwise coordinate, $\frac{2y}{b}$

Subscripts

p potential

v vortex

β partial derivative of the quantity subscripted with respect to β, $\frac{\partial(\ )}{\partial\beta}$, per degree.

MODEL DESCRIPTION, TESTS AND CORRECTIONS

Figure 1 presents a planform sketch of the flat and dihedral configurations used in the present study. The anhedral configuration is obtained by inverting the dihedral configuration. The model was constructed of 1/2 inch aluminum plate and fiberglass. Section I, made of aluminium, is common to all configurations. Section II, also of aluminium and Section III, made of fiberglass, are interchangeable wing tips which form the flat and dihedral configurations respectively. The dihedral coordinates shown in figure 1 were those used for model D572-1 in reference 7. Coordinates for the leading edge of the flat wing-tip model are presented in table 1. The selection of this specific planform is explained in the discussion and presentation of results. A photograph of the model planform is presented in figure 2.

Sharp leading and trailing edges were obtained by symmetrically bevelling the upper and lower surfaces for a distance of 1.25 inches from the model edges. The external balance housing was mounted on the lower surface. It was made of steel with a wooden nose fairing. For two of the configurations, a dummy of the balance housing and fairing mounted on the upper surface, was used to obtain model symmetry. Table 2 presents a summary of the configurations studied. Photographs of several model configurations mounted in the tunnel are shown in figures 3, 4 and 5. The model configurations were painted white for better photographic results and to insure better contrast during the oil flow studies.

The present study was conducted in the NASA Langley high-speed 7- by 10-foot wind tunnel. The forces and moments were measured by a six component strain gage balance mounted externally to the lower surface. Force tests were conducted at a Mach number of 0.165. The angle of attack range was from -4° to 30° and was limited by model buffetting. Sideslip angles were 0° and 5°. Oil flow photographs were taken at 4°, 8°, 16° and 24° angle of attack.

Drag data were corrected for the balance housing base pressure but not for the chamber pressure. Although absolute drag levels will be in error, comparisons between configurations should still be valid.

DISCUSSION AND PRESENTATION OF RESULTS

The present slender wing model is similar to the D572-1 model of reference 7. However, some modifications in the leading-edge sweep were made based on the leading-edge section suction coefficient (c_s) distribution across the semispan. Several planform geometries were analyzed using the vortex lattice program of reference 8 in an attempt to obtain a constant distribution of the section suction coefficient across the semispan. This approach was used since it tends to provide full sweep benefit near the leading edge for the high subsonic cruise condition where attached flow is desired. It must be kept in mind however that for the vortex lift studies of this paper, no attempt was made to provide attached flow at cruise attitudes. Figure 6 presents the section suction coefficient distribution for the planform studied. Although there is some variation in the η = .2 to η = .6 region, the distribution is fairly constant at a c_s value of .375.

Figure 7 presents the $c_s c/2b$ distribution. The peak value occurs inboard at an η of .225. It has been suggested (reference 2) that triangularizing this distribution by moving the peak value as far outboard as possible will, in the separated flow case, delay vortex bursting at the trailing edge until higher angles of attack are obtained. The helium bubble studies of reference 5 show that vortex bursting is delayed the more triangular the $c_s c/2b$ distribution.

Since the primary design parameter is a constant section suction coefficient distribution, no attempt could be made to triangularize the

$c_s c/2b$ distribution. However, explanation of experimental versus theoretical discrepancies appears to involve a more complicated flow phenomenon and interaction than just vortex bursting. As can be seen in the following oil flow study photographs, there appears to be a complex flow system involving two leading edge vortices.

Oil Flow Study

The results of the oil flow study are presented in figures 8 to 15. The effect of the dummy housing on the surface flow of the dihedral model at $\alpha = 24°$, $\beta = 0°$ is shown in figures 8 and 9. In both cases, (dummy off, dummy on) there is no major difference in the oil flow patterns near the edges. The main leading edge vortex is plainly visible with the reattachment line located along the model centerline. A second vortex is located on the wing-tip sections. The dark, hazy lines running along the leading edges are indications of oil pooling. This may be due to flow stagnation along the edges of the vortices.

Figures 10, 11 and 12 are the anhedral, flat and dihedral wing tip models respectively at $\alpha = 16°$, $\beta = 0°$. There appears to be little, if any, change in the main vortex location between these configurations. A flow visualization study employing a method such as a vapor or smoke screen is needed to identify the true vortex behavior. Because of the similarity of the flow patterns, little change in the amount of vortex lift between the three configurations is expected.

Figures 13, 14 and 15 present oil flow results for the flat, anhedral and dihedral cases respectively at $\alpha = 16°$ and $\beta = 5°$. In each case,

the windward wing has a well defined leading-edge vortex system. As in the $\beta = 0^\circ$ cases, there appears to be very little difference between the three configurations.

Longitudinal Aerodynamic Characteristics

The effect on the longitudinal aerodynamic characteristics caused by the variation in wing tip dihedral is presented in figures 16 to 21. Comparisons between theory and data are presented. All theoretical values were obtained using the method of reference 8.

Figures 16 and 17 show the effects of the dummy housing on lift and drag respectively at $\beta = 0^\circ$ for the flat and dihedral wing tips. As expected from the oil flow study, there is very little change in the lift or drag results until an angle of attack of approximately 28° is reached. As a result, succeeding data presented will be for configurations without the dummy housing. This shall apply for the lateral aerodynamic data also, although, the dummy housing would have a more pronounced effect for this kind of flow.

Comparisons of theoretical and experimental lift results for the flat, dihedral and anhedral wing-tip models are shown in figure 18. Theory predicts that the highest total lift (potential plus vortex) is developed by the dihedral case with the next highest by the anhedral configuration. The least amount of lift is predicted for the flat tip configuration. Experimental results, however, show that while the anhedral model develops more lift than does the flat tip model, the dihedral case

produces the least. This could be due to an adverse pressure distribution developing on the dihedral tips resulting in a decreasing velocity on the upper surface. This would result in decreased lift and possibly early vortex bursting. In the same manner, the increase of lift for the anhedral model could be explained by a favorable pressure distribution for the vortices.

Figure 18 also shows that in all three cases, the experimental values fall below the theory. This may be due to the $c_s c$ distribution for this particular planform. Another consideration is the reduced amount of flow reattachment due to the trailing-edge notch effect (see reference 2). Further study of configurations that have variable leading-edge sweep angles and notch ratios is needed to explain the discrepancies between theory and experiment.

Experimental results for the drag and pitching moment are compared with theory in figures 19 and 20 respectively. The theory overpredicts the experimental drag which is to be expected since the lift is overpredicted and the vortex drag is a function of lift and angle of attack.

Figure 21 indicates that for all three cases, the expected pitch-up trend occurs at low angles of attack. For the dihedral and flat wing-tip configurations, this occurs around 9° while for the anhedral configuration it is delayed until 12°. Results for a center of gravity location similar to that of reference 7 are presented in reference 9.

Lateral Aerodynamic Characteristics

The lateral derivatives C_{l_β}, C_{n_β} and C_{Y_β} are presented in figure 22. From the C_{l_β} curve it is seen that for the flat wing tips, the

windward wing lift dominates resulting in a negative C_{l_β}. Because of the positive dihedral of configuration III, it is to be expected that the C_{l_β} as is shown in figure 22 would be more negative than for either the flat or anhedral configuration.

The C_{n_β} plot in general, exhibits positive values over the alpha range. This is due to the windward wing having a higher lift than the leeward wing. Since the induced drag is a function of the lift, then the drag will also be higher on the windward wing. This will result in a positive C_{n_β}.

CONCLUDING REMARKS

The effect of the wing-tip dihedral on the aerodynamic characteristics of a supersonic cruise fighter configuration has been investigated in the NASA Langley high-speed 7- by 10-foot wind tunnel. Both the force and moment data and the oil flow studies show little difference in the general characteristics of the three configurations studied. While large amounts of vortex lift were developed, the full theoretical levels were not reached due to a number of factors including flow interactions, vortex development and notch effect.

Longitudinal force results indicated little difference between the three cases. The anhedral model exhibited some improvements in lift and pitching moment. Lateral force data trends were similar for all three cases. However, the results indicate that a more detailed investigation is needed in order to more fully understand the flow fields

and resulting aerodynamic characteristics of the dihedral and anhedral configurations.

REFERENCES

1. Polhamus, Edward C.: A Concept of the Vortex Lift of Sharp-Edge Delta Wings Based on a Leading-Edge-Suction Analogy. NASA TN D-3767, 1966.

2. Lamar, John E.: Some Recent Applications of the Suction Analogy to the Vortex Lift Estimates. NASA TM X-72785, 1976.

3. Scantling, W. L.; and Gloss, B. B.: Effect of Spanwise Blowing on Leading-Edge Vortex Bursting of a Highly Swept Aspect Ratio 1.18 Delta Wing. NASA TM X-71987, 1974.

4. Erickson, Gary E. and Campbell, James F.: Flow Visualization of Leading-Edge Vortex Enhancement by Spanwise Blowing. NASA TM X-72702, 1975.

5. Washburn, Karen E. and Gloss, Blair B.: The Effect of Wing Dihedral and Section Suction Distribution on Vortex Bursting NASA TM X-72745, 1975.

6. Earnshaw, P. B.: Measurements of Vortex Breakdown Position at Low Speed on a Series of Sharp-Edged Symmetrical Models. C.P. No 828, 1965.

7. Goebel, T. P. and Sitar, M. D.: Analysis of Low Speed Wind Tunnel Test of a D572-1 Supersonic Cruise Vehicle. NA-74-846 Los Angeles Aircraft Division, Rockwell International, 1974.

8. Lamar, John E. and Gloss, Blair B.: Subsonic Aerodynamic Characteristics of Interacting Lifting Surfaces with Separated Flow Around Sharp Edges Predicted by a Vortex-Lattice Method. NASA TN D-7921, September 1975.

9. Campbell, J. F.; Gloss, B. B. and Lamar, J. E.: Vortex Maneuver Lift for Super-Cruise Configurations. NASA TM X-72836, February 1976.

TABLE 1. LEADING EDGE COORDINATES

x (inches)	y (inches)
0.0	0.0
2.708	0.607
5.417	1.083
10.833	1.950
16.250	2.730
18.958	3.088
21.667	3.521
24.375	4.063
27.083	4.950
28.438	5.471
31.146	6.771
32.500	7.583
33.854	8.531
35.208	9.714
36.563	10.901
37.375	11.613
38.729	12.634
39.542	13.000

NOTE: x IS MEASURED FROM NOSE OF MODEL.
y IS MEASURED FROM MODEL CENTERLINE.

TABLE 2. CONFIGURATION DEFINITION

CONFIGURATION	WING TIP	DUMMY
I	FLAT	OFF
II	FLAT	ON
III	ARC DIHEDRAL	OFF
IV	ARC DIHEDRAL	ON
V	ARC ANHEDRAL	OFF

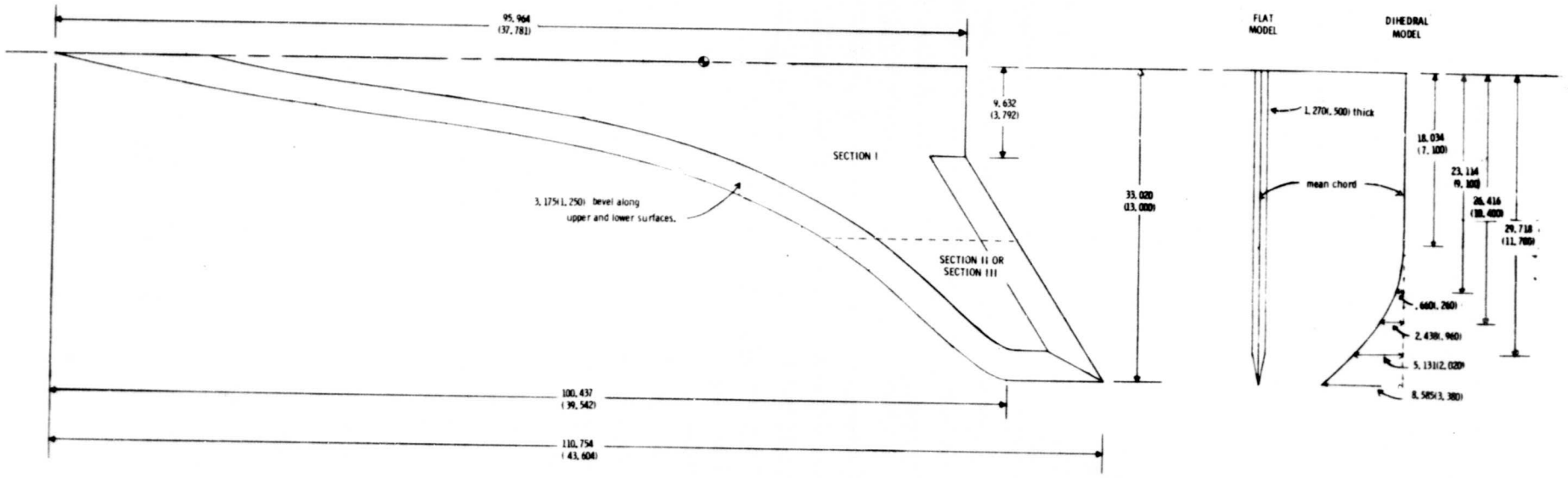

FIGURE 1. MODEL DRAWING - DIMENSIONS IN cm. (In.).

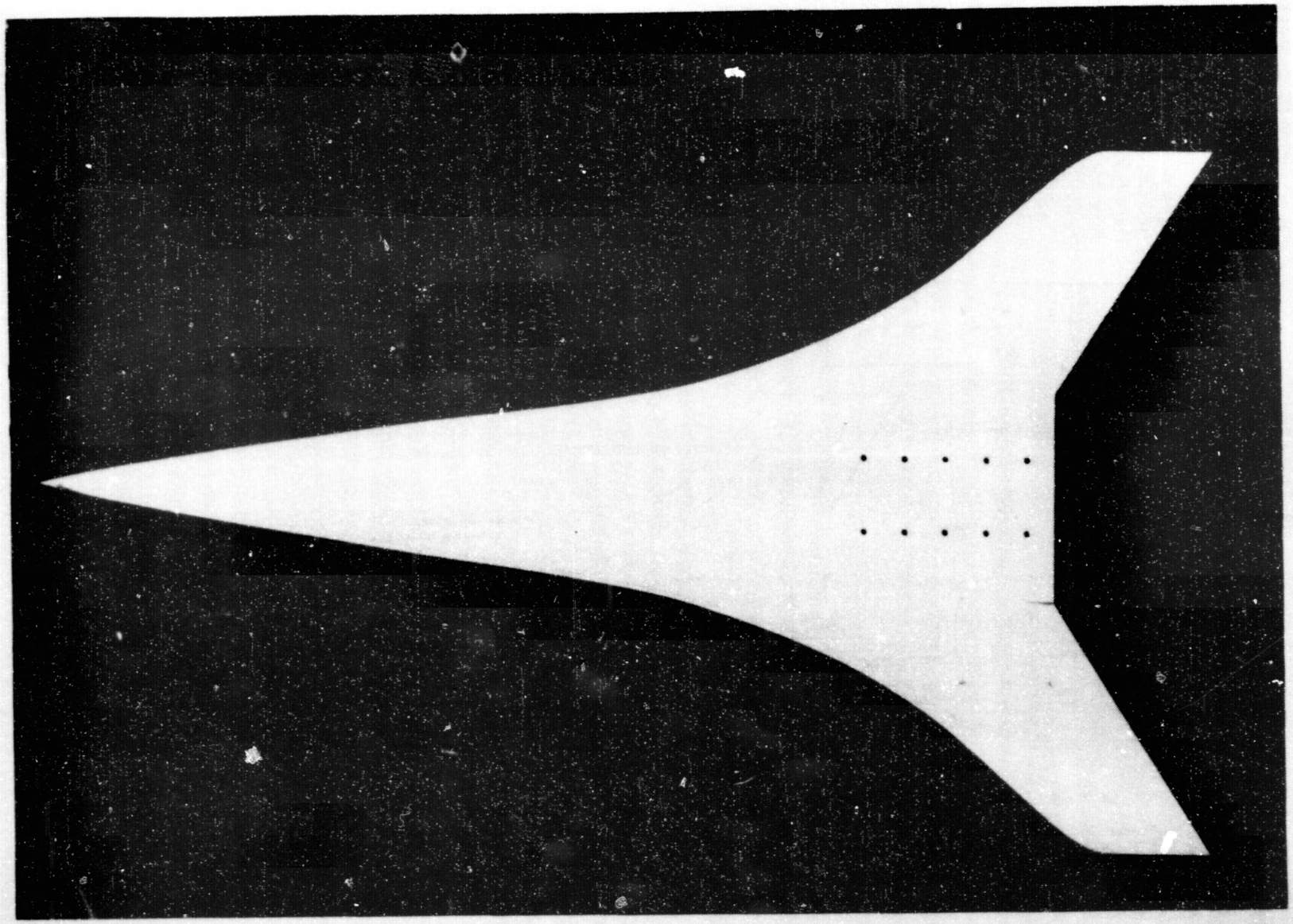

FIGURE 2. SUPERSONIC CRUISE FIGHTER MODEL PLANFORM.

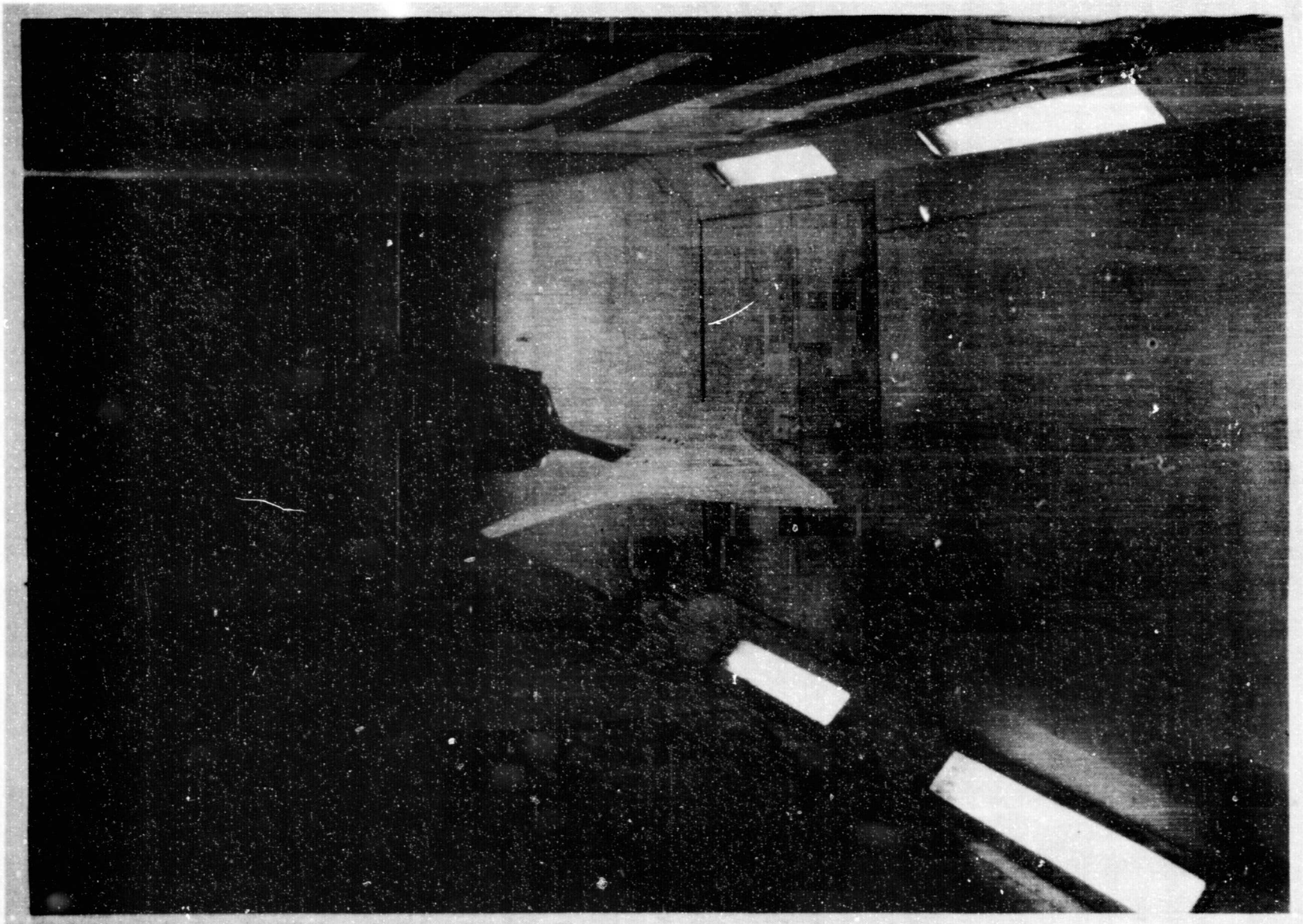

FIGURE 3. CONFIGURATION I MOUNTED IN TUNNEL.

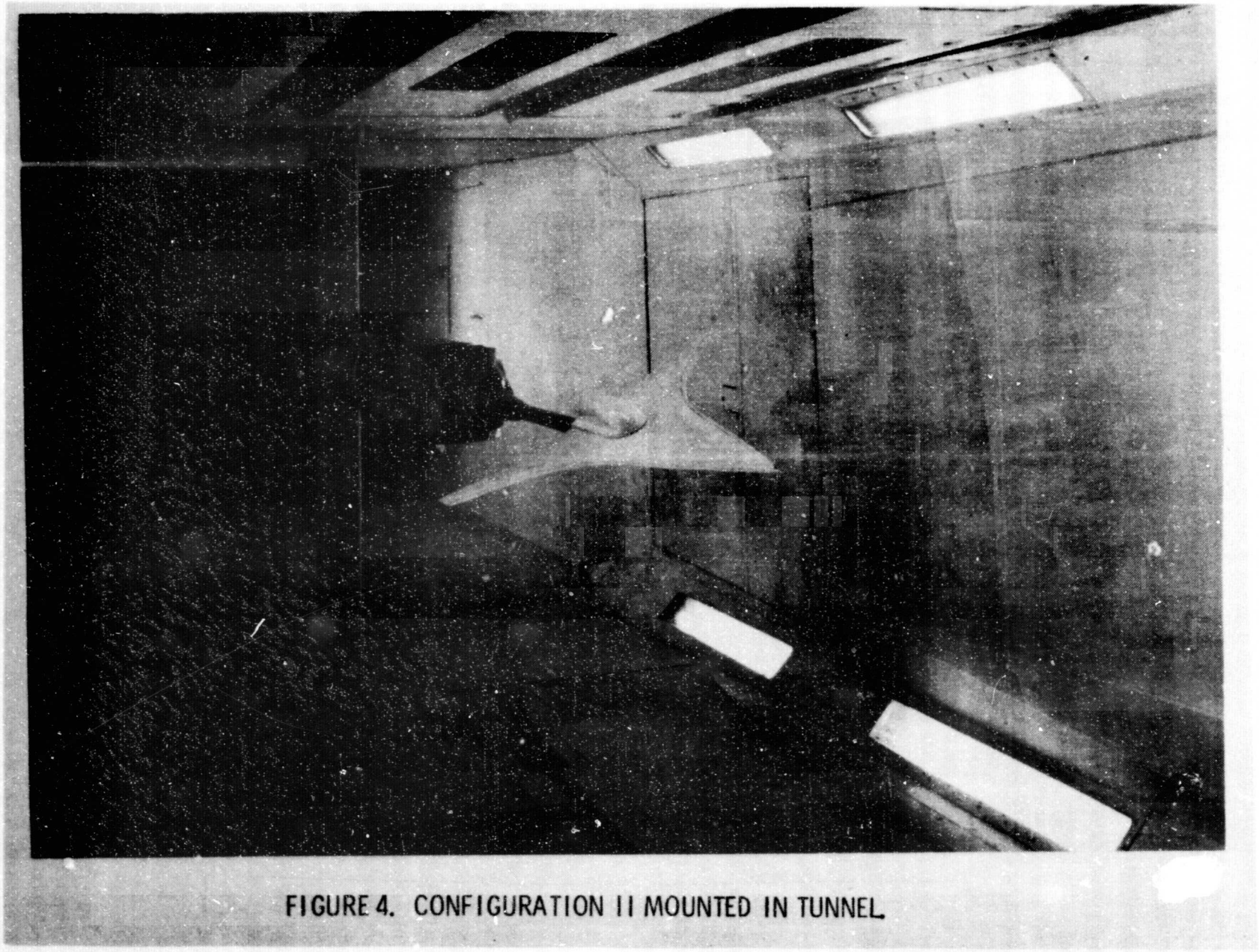

FIGURE 4. CONFIGURATION II MOUNTED IN TUNNEL.

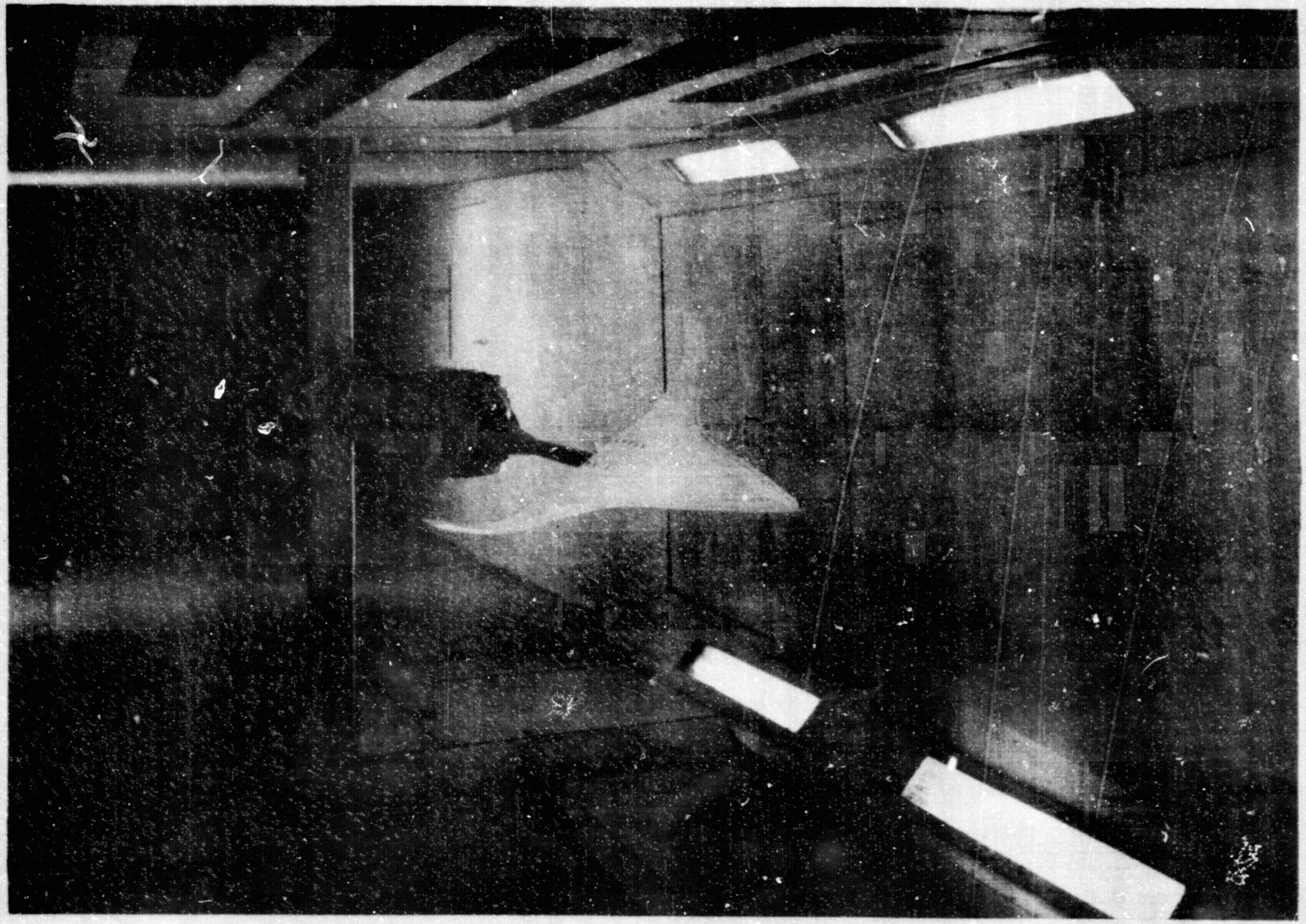

FIGURE 5. CONFIGURATION III MOUNTED IN TUNNEL.

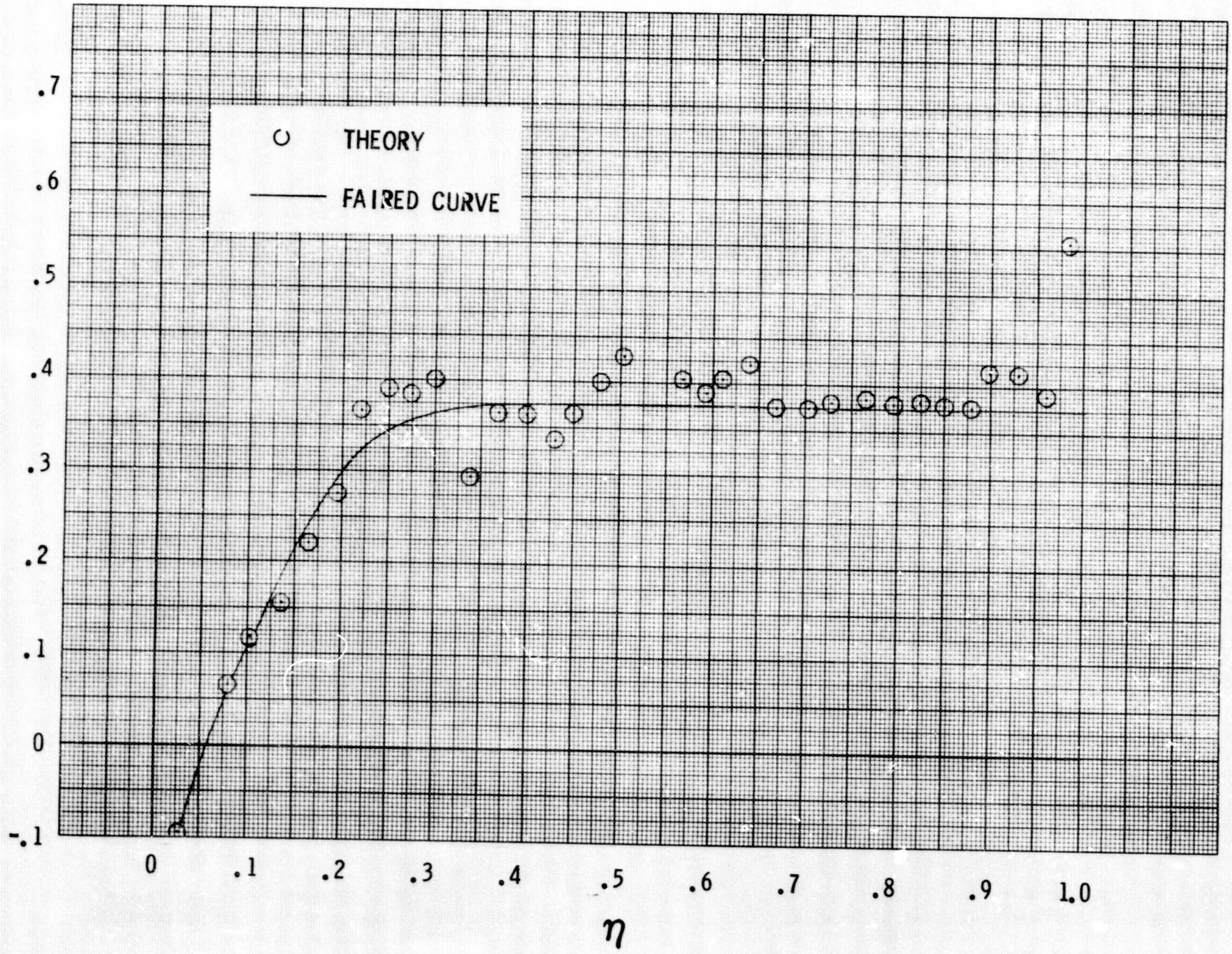

FIGURE 6. SECTION SUCTION DISTRIBUTION FOR THE FLAT WING TIP MODEL.

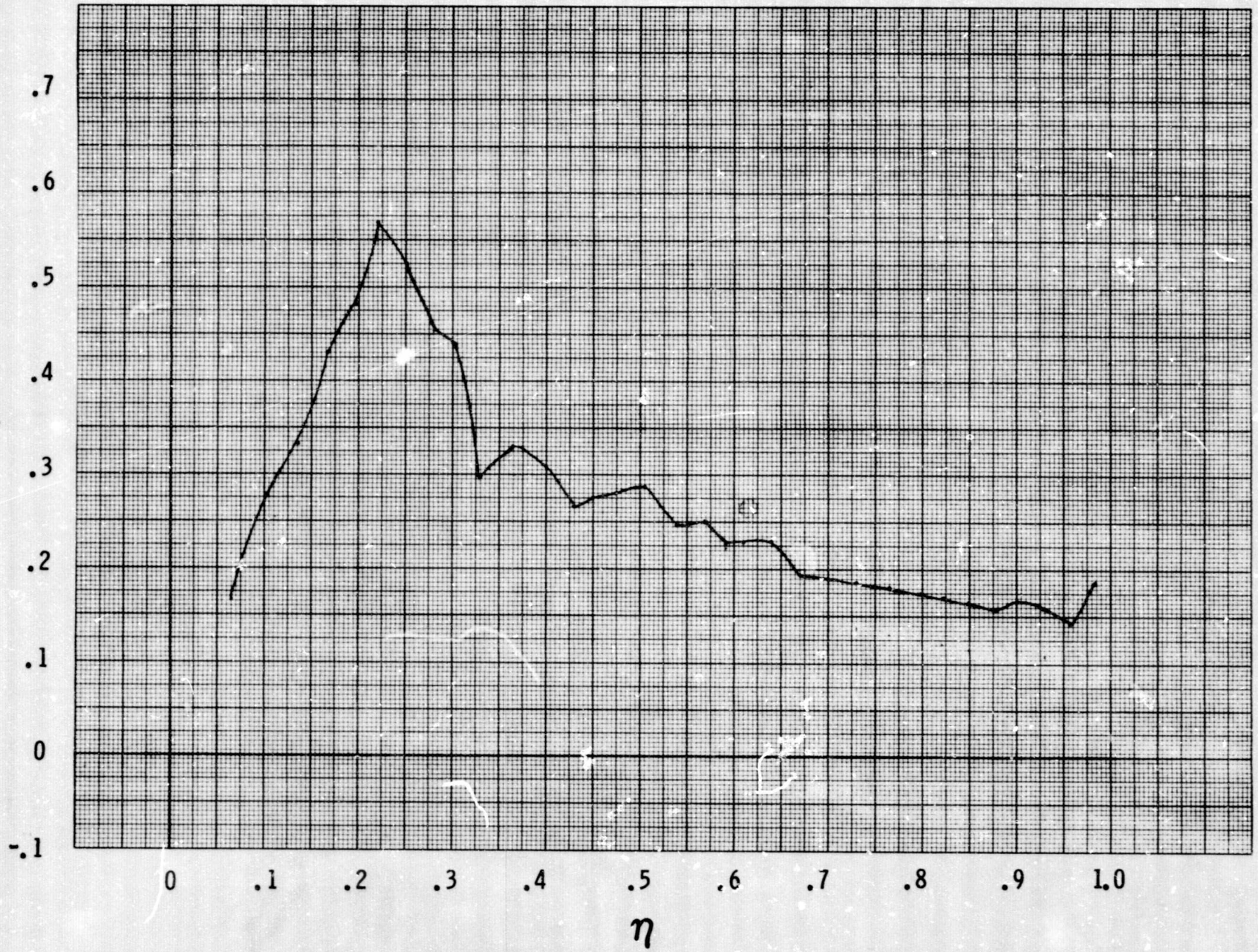

FIGURE 7. $\frac{C_s C}{2b}$ DISTRIBUTION FOR THE FLAT WING TIP MODEL.

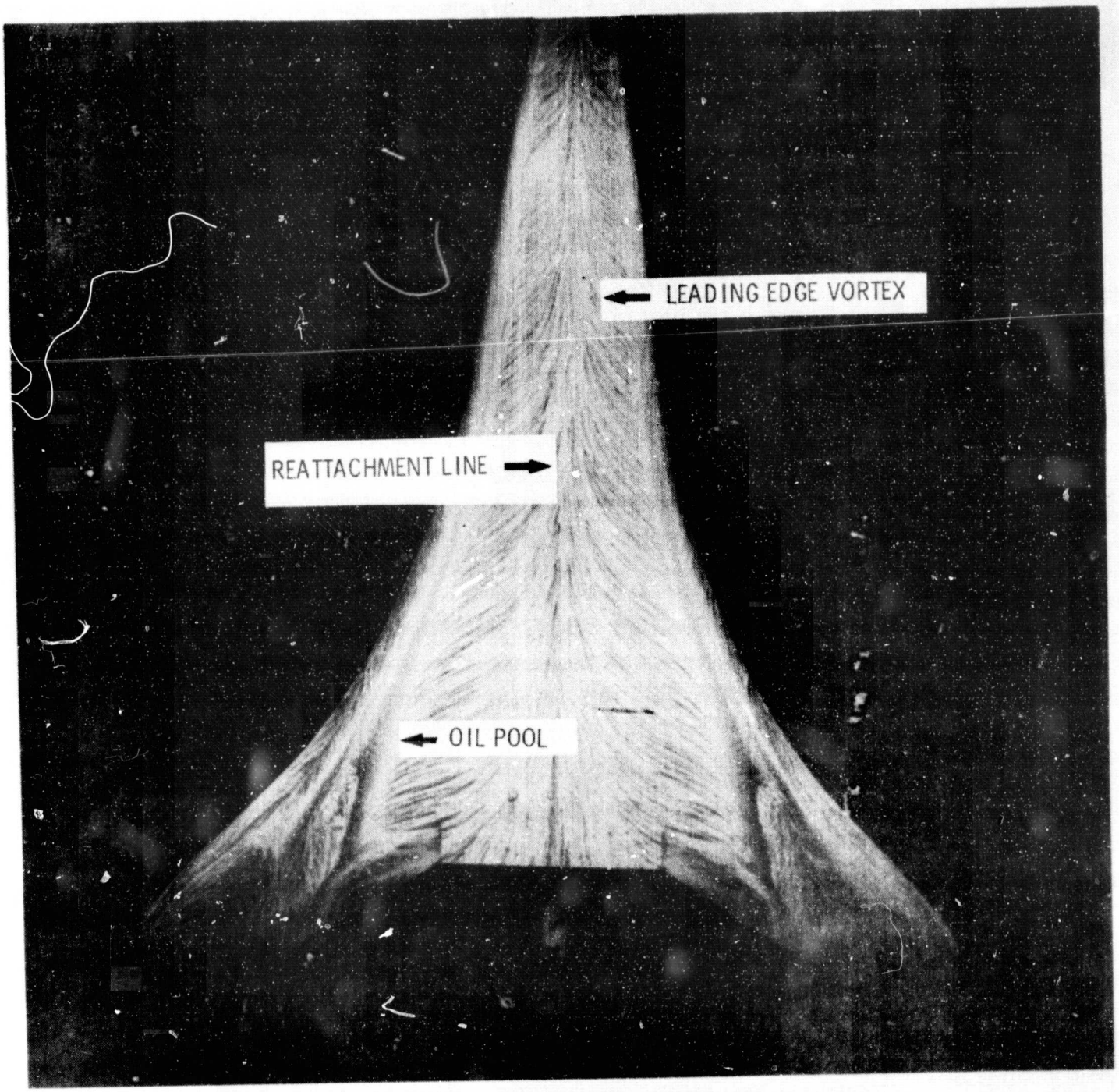

FIGURE 8. DIHEDRAL MODEL AT $\alpha = 24^{\circ}$, $\beta = 0^{\circ}$.

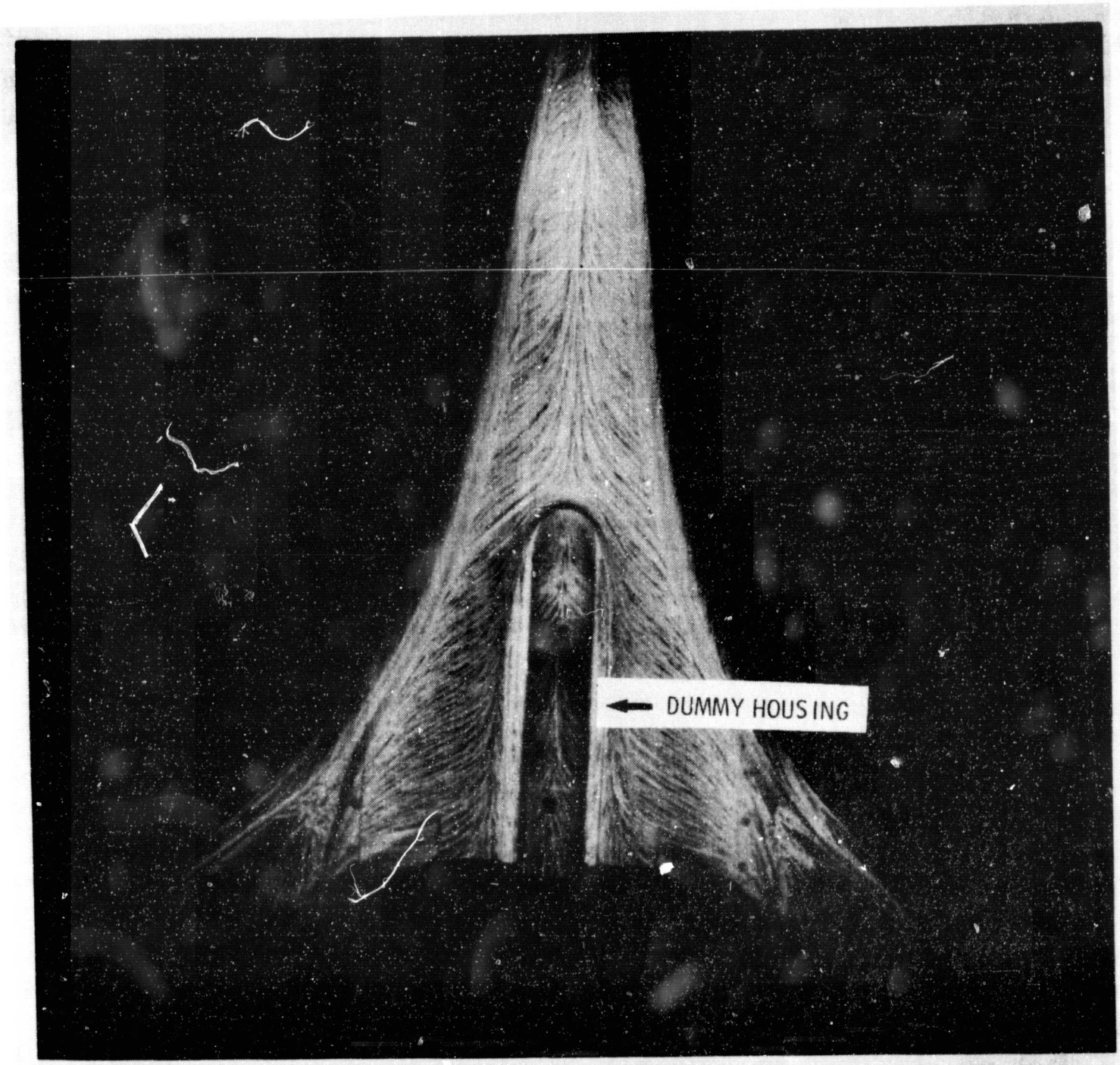

FIGURE 9. DIHEDRAL MODEL WITH DUMMY AT $\alpha = 24^{o}$, $\beta = 0^{o}$.

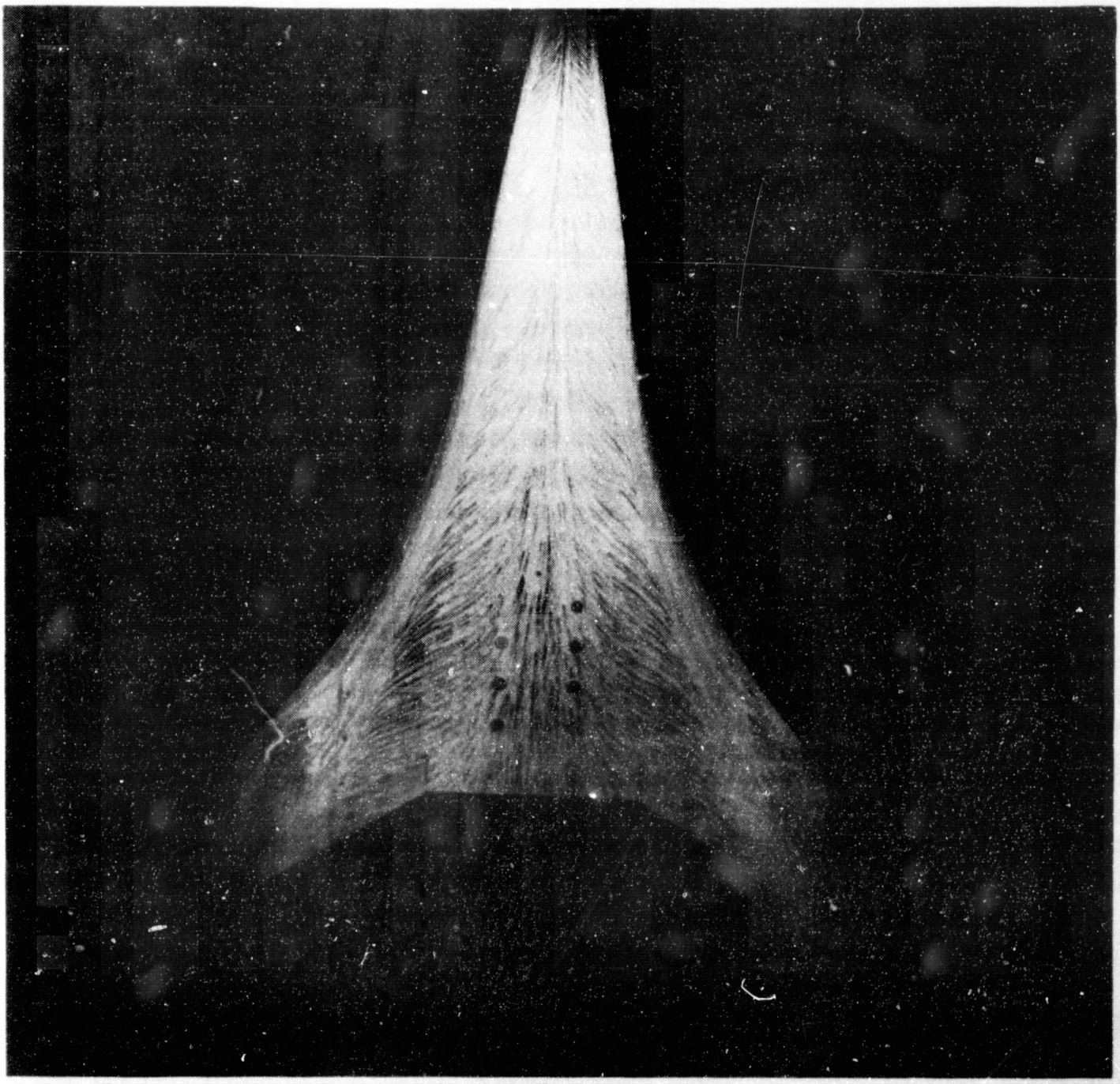

FIGURE 10. ANHEDRAL MODEL AT $\alpha = 16^{0}$, $\beta = 0^{0}$.

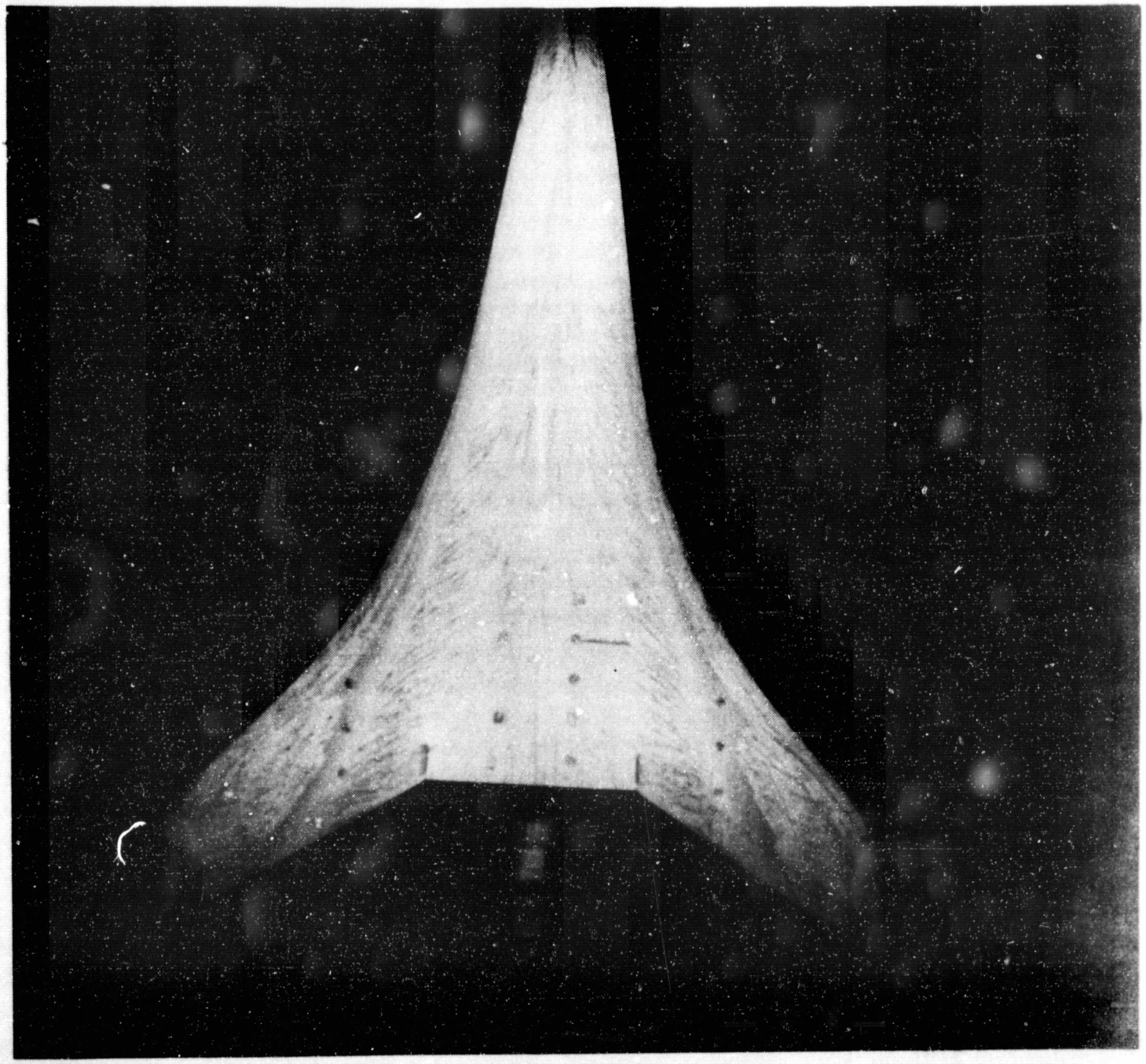

FIGURE 11. FLAT WING TIP MODEL AT $\alpha = 16^{0}$, $\beta = 0^{0}$.

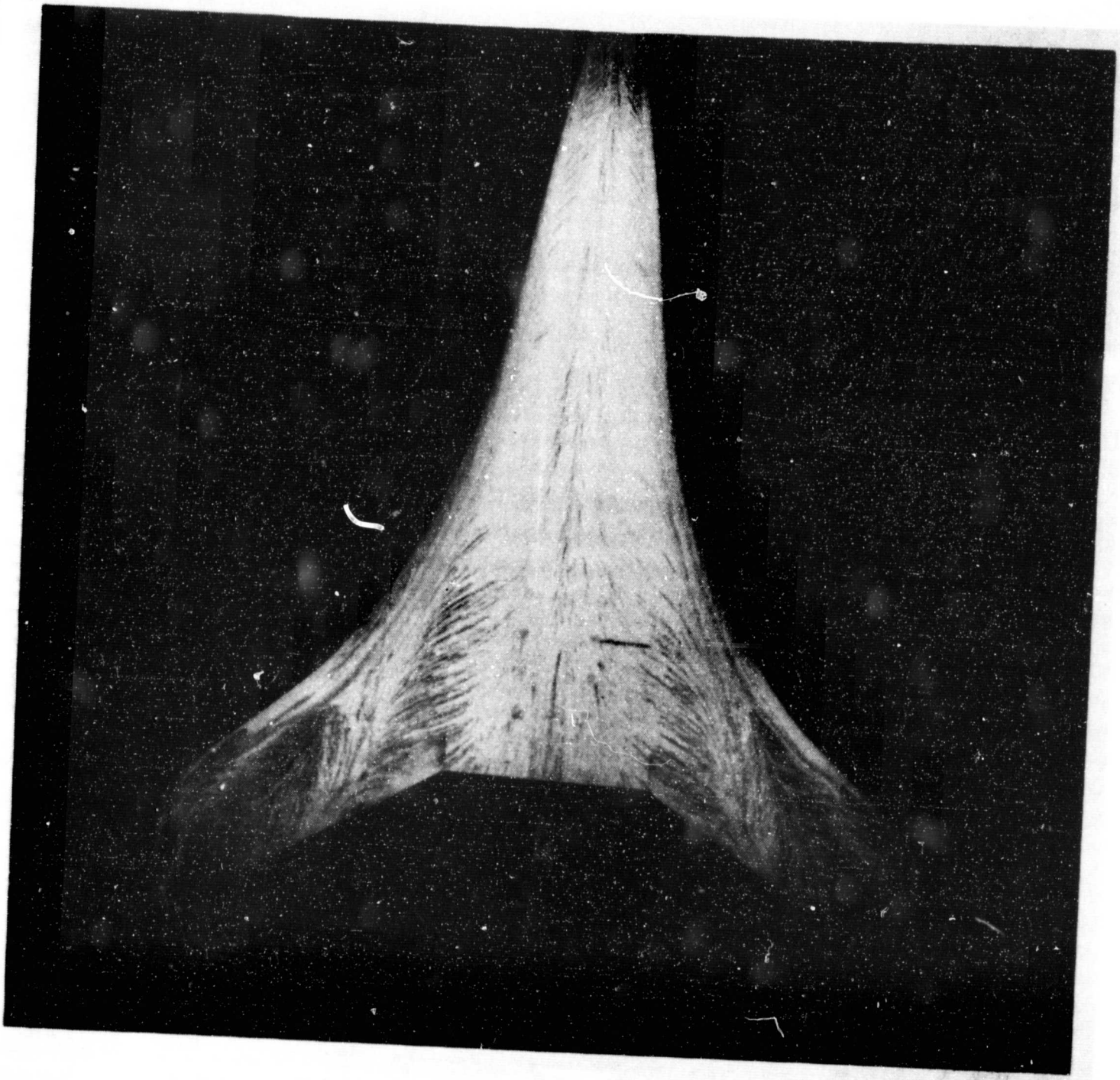

FIGURE 12. DIHEDRAL MODEL AT $\alpha = 16^{0}$, $\beta = 0^{0}$.

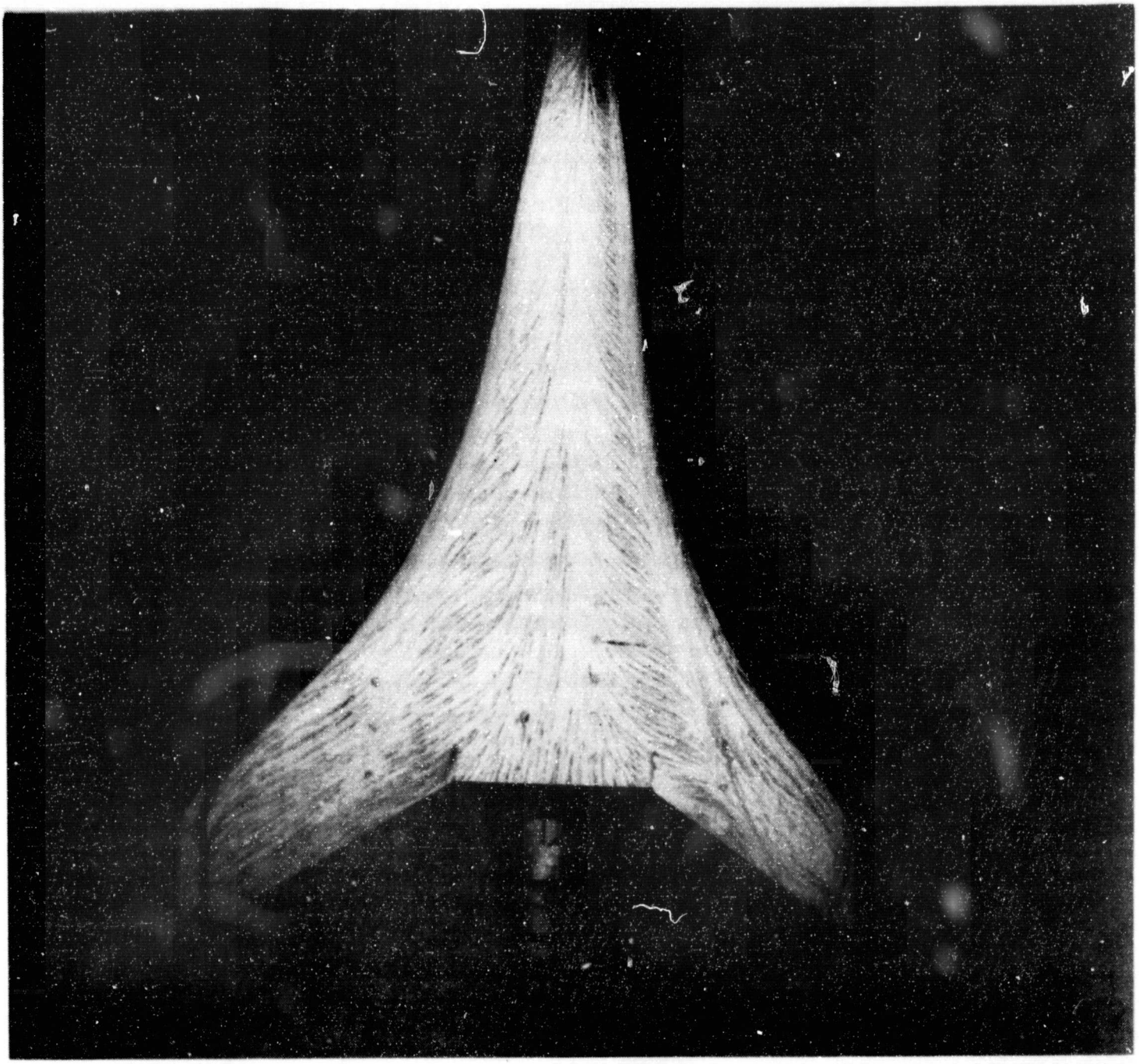

FIGURE 13. FLAT WING TIP MODEL AT $\alpha = 16^0$, $\beta = 5^0$.

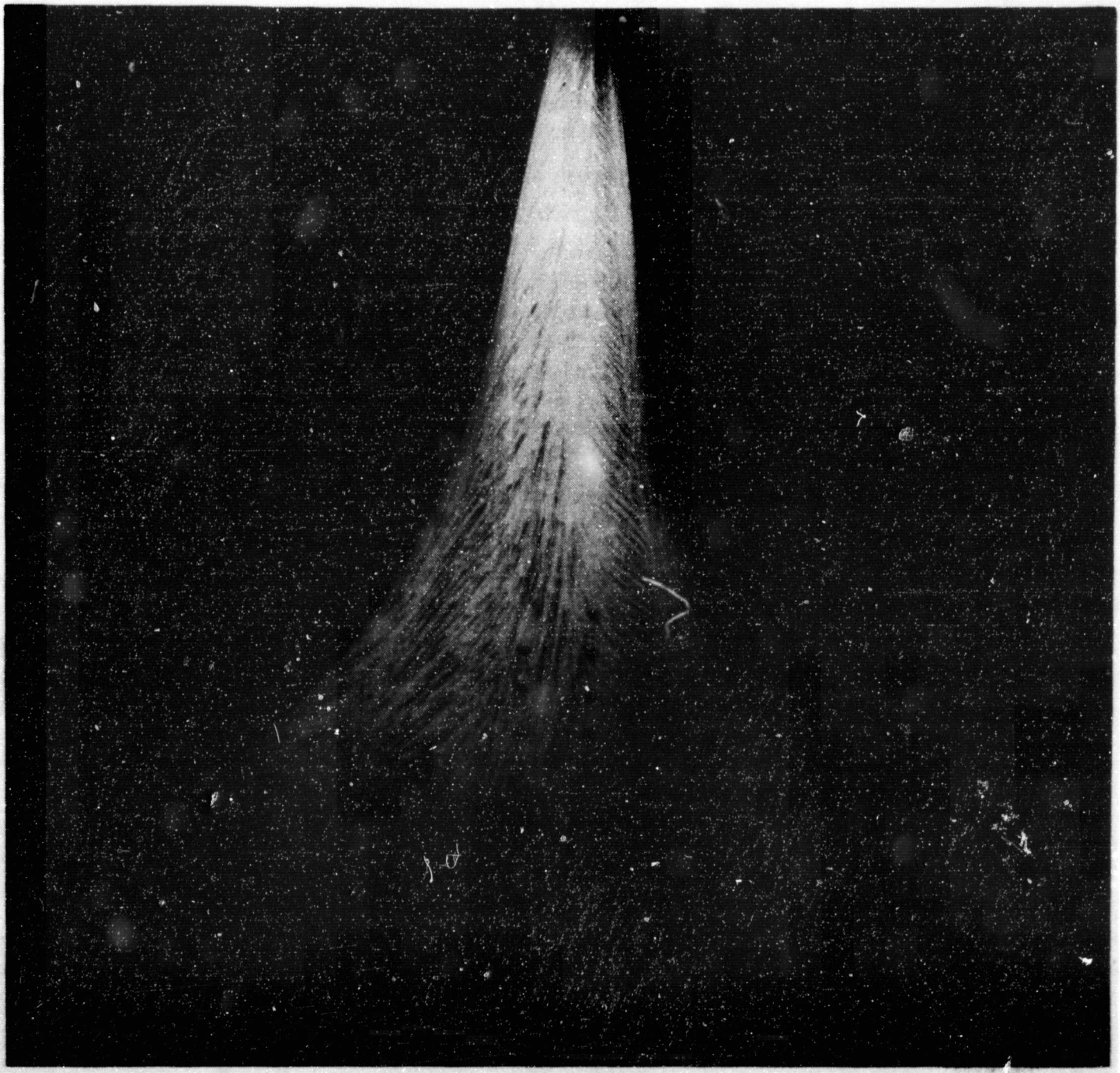

FIGURE 14. ANHEDRAL MODEL AT $\alpha = 16^{0}$, $\beta = 5^{0}$.

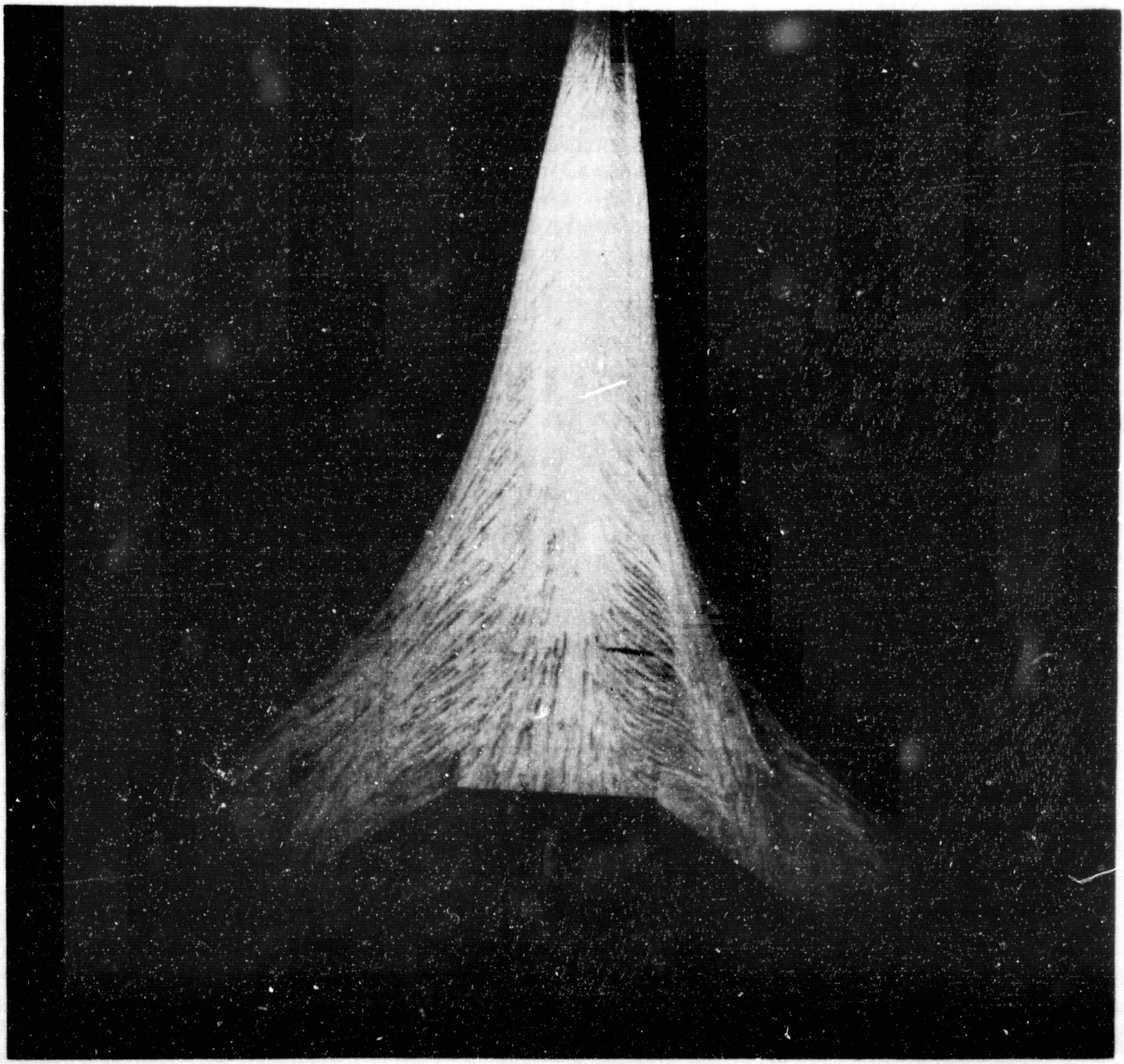

FIGURE 15. DIHEDRAL MODEL AT $\alpha = 16^{0}$, $\beta = 5^{0}$.

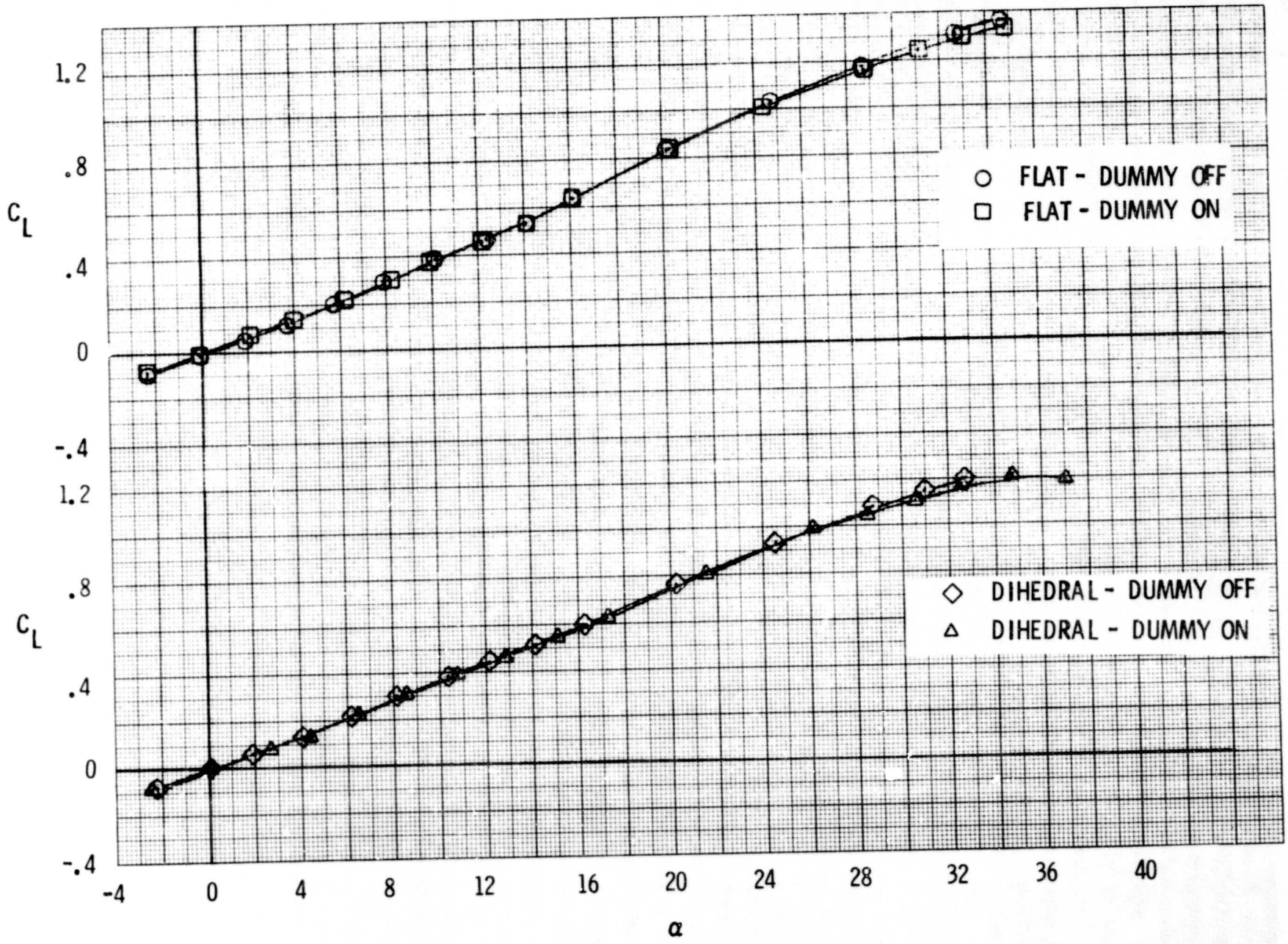

FIGURE 16. EFFECT OF DUMMY HOUSING ON LIFT, $\beta = 0^0$.

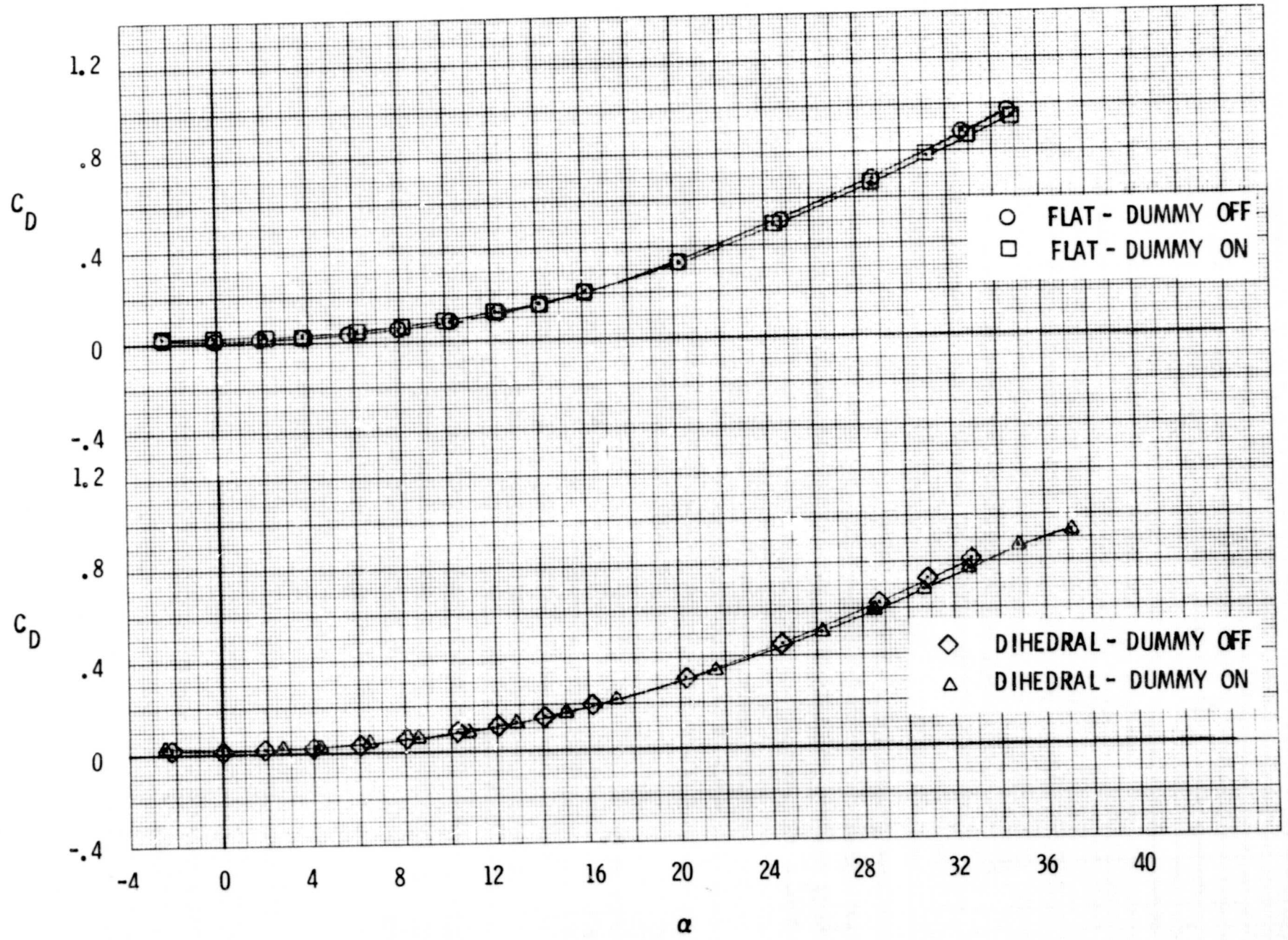

FIGURE 17. EFFECT OF DUMMY HOUSING ON DRAG, $\beta = 0^0$.

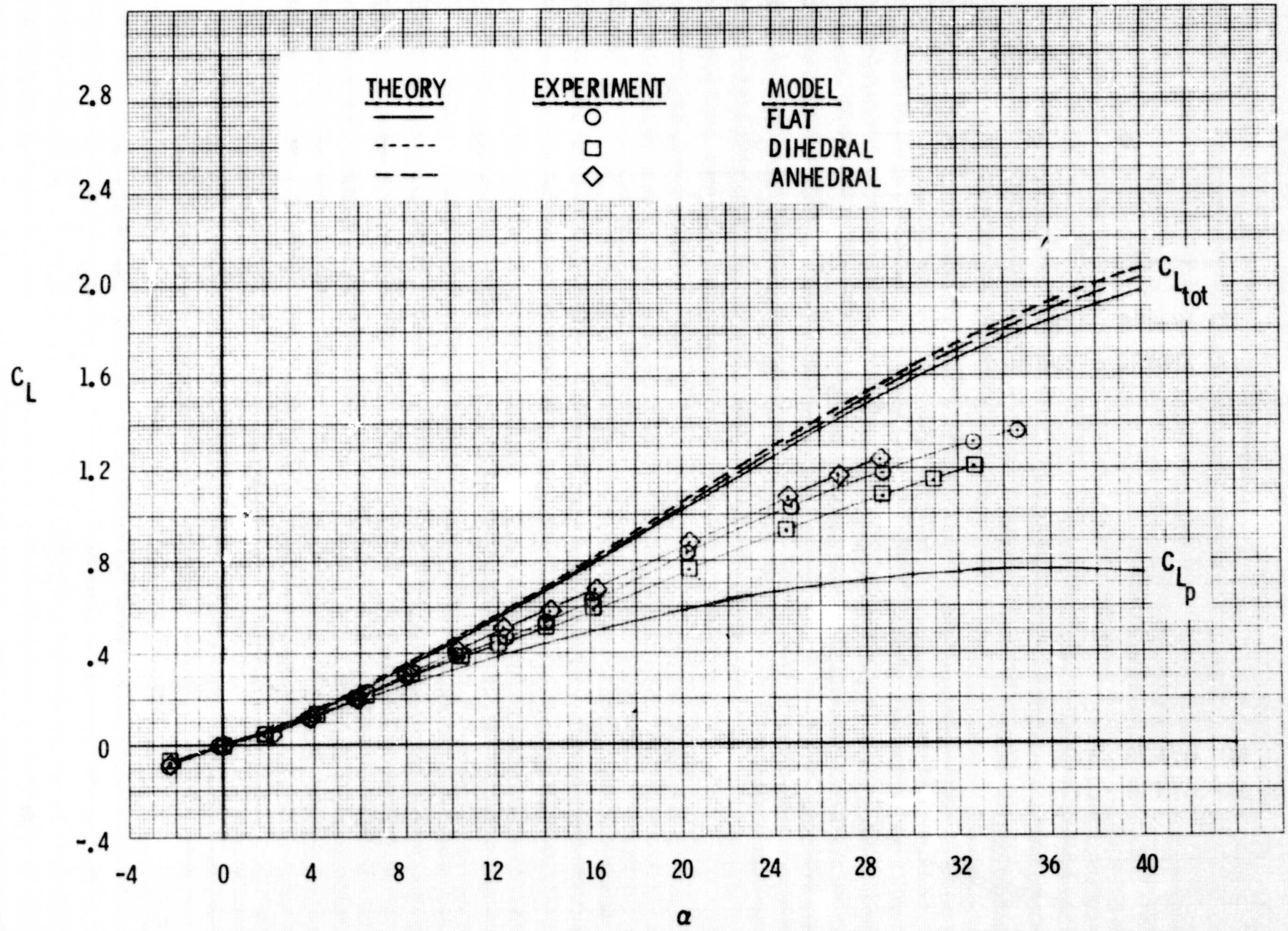

FIGURE 18. THEORETICAL AND EXPERIMENTAL LIFT COMPARISONS , $\beta = 0^0$.

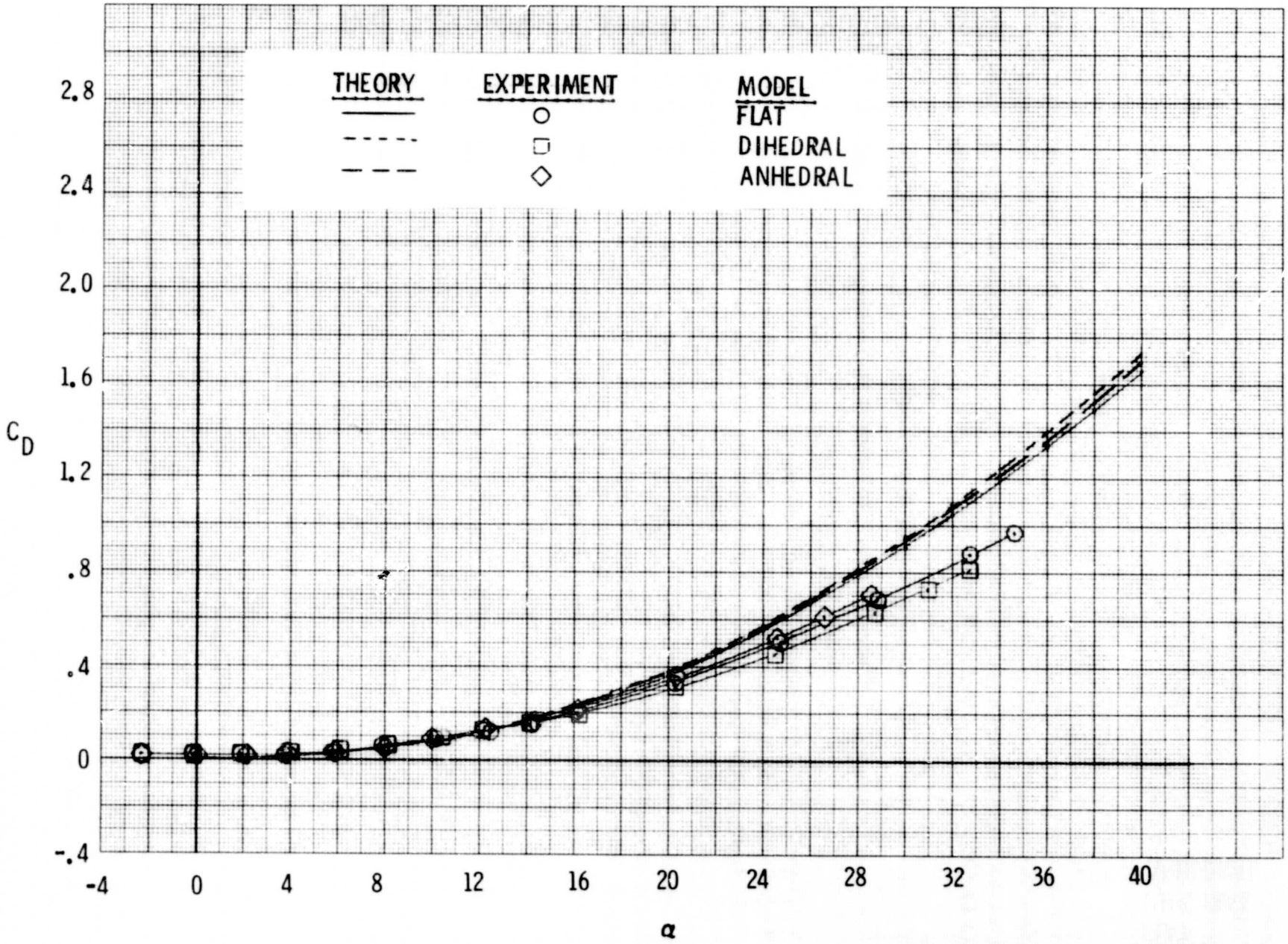

FIGURE 19. THEORETICAL AND EXPERIMENTAL DRAG COMPARISONS, $\beta = 0^0$

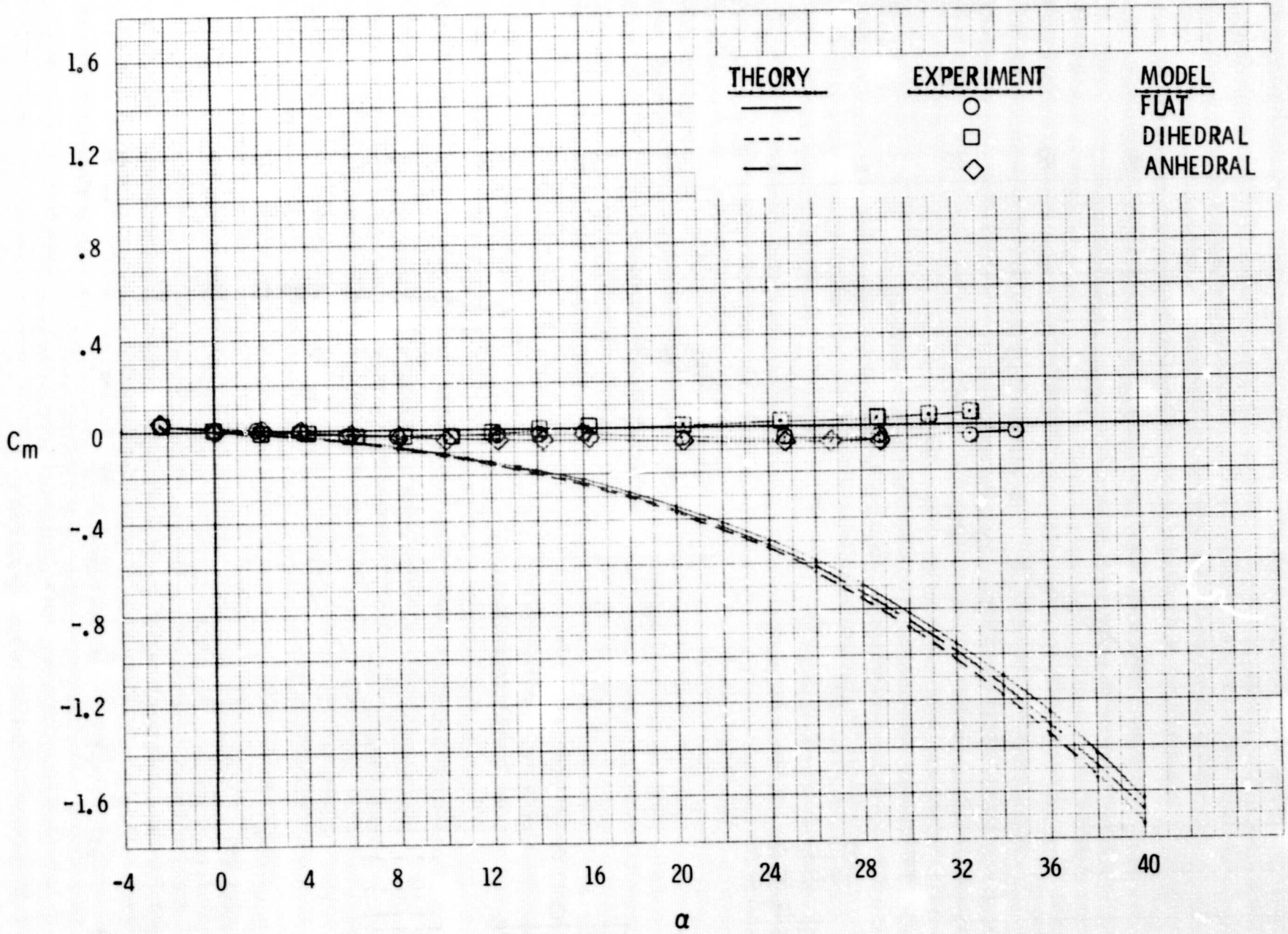

FIGURE 20. THEORETICAL AND EXPERIMENTAL PITCHING MOMENT COMPARISONS , $\beta = 0^0$

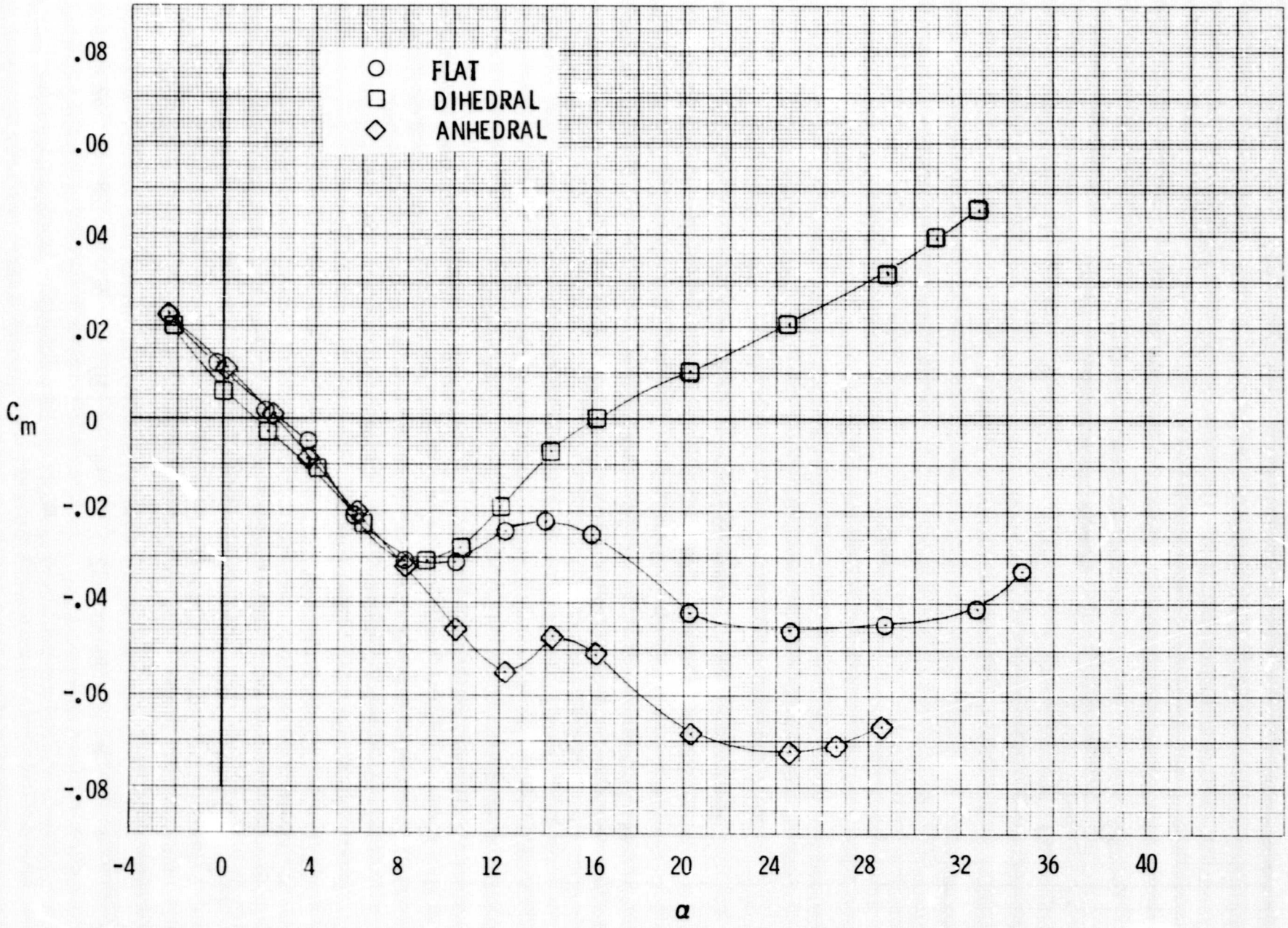

FIGURE 21. EXPERIMENTAL PITCHING MOMENT COMPARISONS , $\beta = 0^0$.

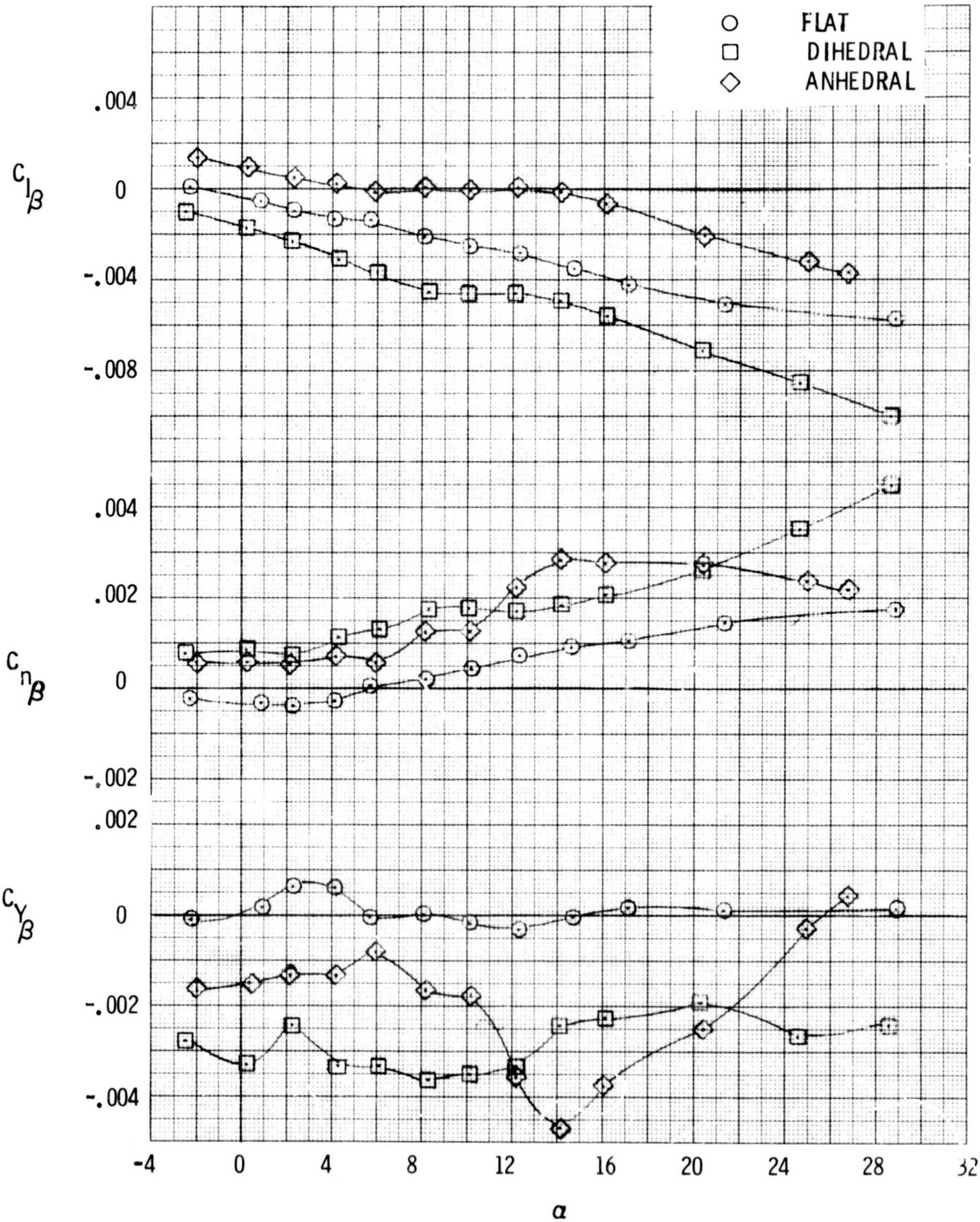

FIGURE 22. LATERAL STABILITY DERIVATIVES.